Tunneling Excitation to Resonant States in Helium as Main Source of Superponderomotive Photoelectrons in the Tunneling Regime

H. G. Muller

FOM-Institute for Atomic and Molecular Physics, Kruislaan 407, 1098 SJ Amsterdam, The Netherlands

(Received 19 April 1999)

We present numerical solutions of the time-dependent Schrödinger equation in the single-active-electron approximation and calculate wave functions for photoionization of helium exposed to 800 nm light. Electron spectra show ~200 peaks up to 272 eV, due to above-threshold ionization. The simulations confirm the existence of a wide, flat plateau in the electron spectrum due to backscattering, between 3 and 8 times the ponderomotive energy. Electrons in this range originate almost exclusively through resonance enhancement by quivering excited states, which in turn are populated by light-induced tunneling from the ground state.

PACS numbers: 32.80.Fb, 31.15.–p

At intensities where the electromagnetic radiation starts to rival the fields that bind the atom together, ionization can occur with an arbitrary number of photons, and as a consequence radiation of any frequency can do the job. The atom then has the tendency to absorb more photons than required to overcome the ionization potential, the excess being converted into kinetic energy of the photoelectron [above-threshold ionization [1] (ATI)].

If the light frequency ω is low on the time scale of electron motion, there is approximate energy conservation with respect to the instantaneous potential created by Coulomb attraction and laser field. This potential features a saddle point, and at high light intensity I it can be pushed down to the energy U_0 of the atomic state [2]. Escape over or tunneling just under this barrier then leads to ionization, hence the name tunneling regime.

At high light frequency the electron takes several cycles to move significantly, and cycle-averaged energy quantities dominate its dynamics. Even with respect to the average potential energy there is no energy conservation: electrons gain kinetic energy by "bouncing around" in a time-dependent potential well and can derive enough kinetic energy from this to escape the well. This regime is known as the multiphoton regime.

Keldysh [3] has proposed a quantitative measure $\gamma = \sqrt{|U_0|/2U_p}$ to decide which description is applicable. Here $U_p = I/4\omega^2$ [4] is the ponderomotive energy [5]. If $\gamma \ll 1$ the tunneling picture is applicable, while $\gamma \gg 1$ in a typical multiphoton case [6]. Ionization of helium at wavelength $\lambda = 800$ nm [7] is one of the few cases that is fairly deep in the tunneling regime [8], with $\gamma \approx 0.5$.

Tunneling and multiphoton ionization are limiting cases of the same basic process, and thus share many properties. In monochromatic light, energy exchange with the field can take place in quantized steps of photons. Continuous energy shifts can occur during time intervals where the field changes, through scattering of photons between field modes [9] of different ω. Thus photoelectrons generated during a flat part of a laser pulse will appear with energies an integer number of photons above the Stark-shifted ground state, giving rise to the familiar ATI spectrum of peaks spaced by $\hbar\omega$, both in the multiphoton and the tunneling regime. The periodic repetition of the basic production event ensures this [10].

Experiments so far have not been able to resolve individual ATI peaks in the helium case [7], for practical reasons: U_p is huge (~30 eV) at intensities where the ionization yield becomes detectable. Photoelectrons are perturbed in energy during their escape from the focus by the ponderomotive force [11] as long as the light is on, and the broadening due to this [12] is enough to completely wash out the peak structure even if only a few percent of U_p is involved.

In this paper we study the ionization of helium by numerically integrating the time-dependent Schrödinger equation

$$i\partial t\Psi = \left(\frac{1}{2}\,p^2 - V(r) - A(t)\,p\right)\Psi \qquad (1)$$

in the single-active-electron approximation. The (three-dimensional) potential well used to model the atom is given by

$$V(r) = 1/r + (2 + 1/r)e^{-4r}, \qquad (2)$$

which is the potential of a nucleus of charge 2 screened by the static charge distribution of the He^+ $1s$ orbital. Since the polarizability of the He^+ core is very small, this potential should give a fairly good representation of the electron-core interaction in the region near the saddle point (which at 500 TW/cm^2 occurs around $r = 3$). To mimic the effects of electron correlation (important near the nucleus) we adjusted the potential in the first grid point [13] to obtain the correct U_0 of -0.9036 hartree. This also produces reasonable quantum defects for s states. It hardly affects any of the higher angular momenta, which avoid the nucleus quite strongly.

The model atom was exposed to a 16-cycle flat-top laser pulse $A(t) = A_0\hat{z}\cos\omega t$, with half-cycle turn-on and turn-off [14]. The frequency ω was chosen

 0031-9007/99/83(16)/3158(4)$15.00

as 0.056 957, corresponding to a laser wavelength of 800 nm. Collection of photoelectrons was done during the last six cycles of the pulse only; during the first ten cycles an absorbing wall was put 90 bohr from the nucleus, to absorb virtually all electrons emitted during the turn-on and the transient period immediately following it. The photoelectrons that remained within 1440 bohr from the atom were spectrally analyzed after the pulse. This region is large enough to contain all electrons emitted during collection with energies below 2.5 hartree. Faster electrons have moved partly off the grid so that the calculation underestimates their numbers (by a known amount), but even at 10 hartree the collection efficiency is still 50%. This procedure is an efficient way to obtain the atomic response to a laser beam of constant light intensity.

Integration was done with a velocity-gauge propagation scheme, which was described extensively elsewhere [15,16]. In short, it uses a radial-position/angular-momentum grid to represent the wave function, with a fourth-order implicit finite-difference representation of the radial derivatives. Time integration is done by a unitary half-implicit split-operator scheme that is second order in the time step. To get a reasonable degree of convergence, about 120 angular momenta were required at a radial grid spacing $\delta r = 0.15$ and 2000 time steps per optical cycle.

Figure 1 shows a typical calculated energy spectrum of electrons escaping along the polarization vector. Most spectra in this intensity range have a similar appearance, with comparatively strong ATI peaks in the region 0–2 hartree, and quickly dropping off above that to a wide plateau extending between 3 and 9 hartree. Unlike experiments, the calculations do not suffer from a distribution of intensities causing inhomogeneous broadening, nor is there any ponderomotive acceleration of free electrons in the dipole approximation. As a result, the ATI peaks are well resolved (their width is limited by the 6-cycle collection time through the uncertainty relation). About 160 peaks are visible, sticking out above the continuous background (mostly due to ionization during turn-off) by a factor of 30.

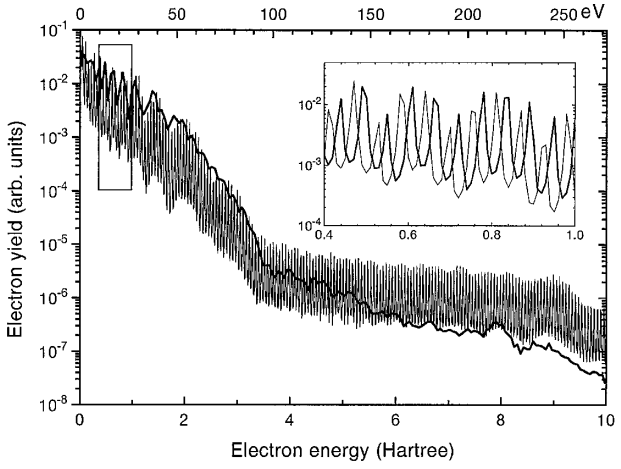

FIG. 1. Calculated ATI spectrum of helium for a 0.1291 a.u. field (585 TW/cm^2) at 800 nm, along the polarization vector. At this intensity there is a strong plateau between 4 and 8 hartree. The fat curve shows the spectrum at a slightly different field (0.1274 a.u.), which is nearly identical at low energy, but has a much weaker plateau. The inset is a blowup of the indicated region, revealing how the ATI peaks shift ponderomotively through a nearly constant envelope. For clarity the main plot shows only the envelope for the fat spectrum.

The strong part of the spectrum below 2 hartree corresponds to classically allowed energies for electrons accelerated by the field after tunneling out of the atom [17,18]. Its envelope shows modulations like those predicted from approximate models [19], in which the ATI amplitudes are given as (generalized) Bessel functions. The plateau lies between $2U_p$ and $10U_p$, the range that is classically accessible to electrons that backscatter from the residual ion after the field has driven them back towards the nucleus [18,20]. Unlike plateaus observed in argon [21–23], the envelope of this plateau is very flat. At slightly different intensities, the low-order part of the spectrum is very similar (the ATI peaks shift ponderomotively through a nearly intensity-independent envelope), but the level of the plateau can be drastically different (Fig. 1).

The production of "superponderomotive" electrons, as derived from integrating the ATI spectrum between 4 and 8 hartree, is plotted as a function of intensity in Fig. 2a. To obtain this plot, the calculation described above was repeated for a few hundred different intensities between 420 and 600 TW/cm^2 (electric field amplitudes $F = \omega A_0 = 0.11$ to 0.13 a.u.). Strong enhancements of the plateau roughly recur each time the intensity is raised enough to increase the ponderomotive shift by $\hbar\omega$. (This makes the plot look like an ATI spectrum, although it is not one at all.) When an integer number of photons equals the Stark-shifted ionization potential [11] $|U_0| + U_p$, the yield in the plateau is very low, with maxima in between. If the threshold is at $\approx(N + 0.5)\hbar\omega$ (i.e., N photons are slightly below threshold) the enhancements occur. This suggests that they are caused by states about $0.5\hbar\omega$ below the threshold, which are ponderomotively scanned through resonant position an integer times $\hbar\omega$ above the ground state [24]. Resonant states reached with even and odd numbers of photons must have opposite parities and thus must be different.

A high-resolution intensity scan shows that even within the recurrence interval more than one resonance occurs (Fig. 2b), and that the pattern of enhancements repeats after U_p is increased by $2\hbar\omega$. The resonance peaks are extremely narrow, nearly at the bandwidth limit of the pulse. This suggest the lifetime of the involved states is similar to the pulse duration of 16 cycles [25].

To identify the responsible states their wave functions were analyzed. To make this possible amidst the strong flux of low-energy electrons, the ground-state population was removed from the wave function near the end

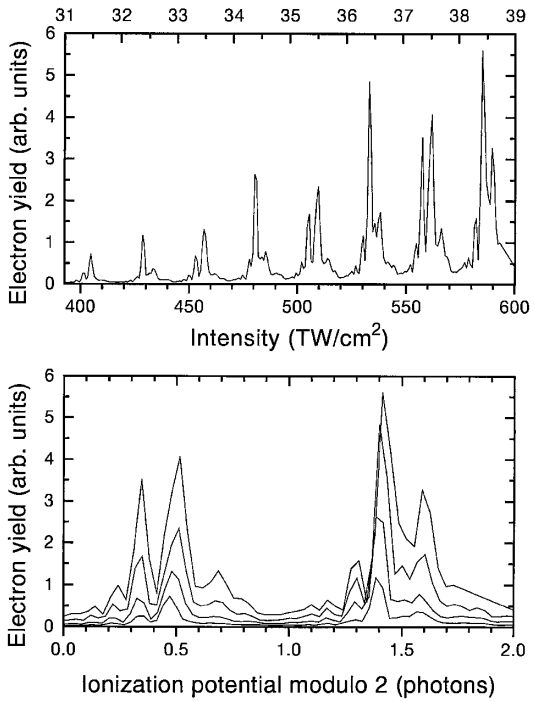

FIG. 2. The yield of electrons in the polarization direction between 4 and 8 hartree ("backscattering") as a function of intensity. The upper plot shows that enhancements occur over the entire intensity range of practical interest. Intensities where channels close are marked by ticks on the upper axis, the associated number indicating with how many photons the particular channel is reached from the Stark-shifted ground state. The lower plot folds the same data into an interval $2\hbar\omega$, clearly showing that even and odd resonance groups are caused by different sets of (interleaved) states.

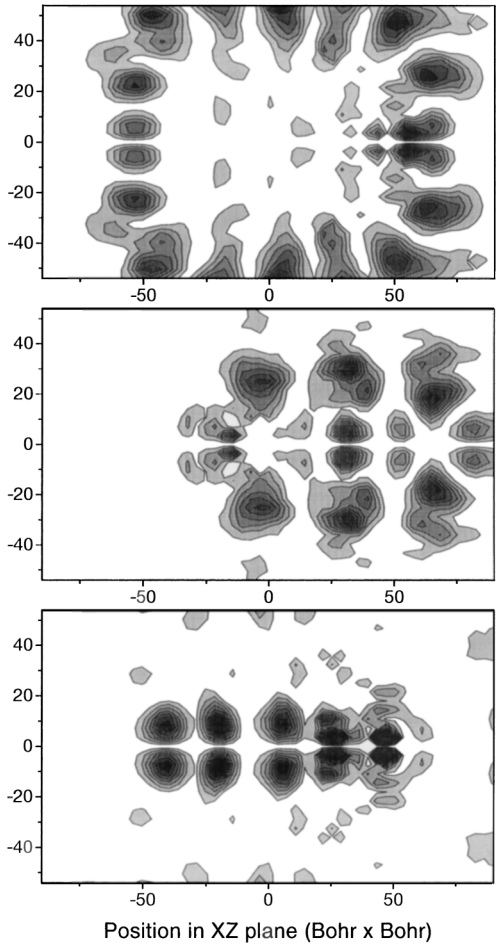

FIG. 3. Contour plots of the charge distributions (multiplied by the cylindrical volume element) of resonant states in a plane through the (horizontal) polarization axis, as revealed after removing ground state and continuum (see text). Field amplitudes for exciting the states (by a 38-photon transition) were (top to bottom) 0.1284, 0.1291, and 0.1296 a.u. In the course of an optical cycle the states move horizontally over ≈40 bohr in either direction, during which the charge distribution shows subtle changes. They are represented here at a phase selected to most clearly exhibit their average features. The "node" on the horizontal axis is entirely due to the volume element, the charge densities themselves all have maxima there.

of the pulse by projection [26], after which 3 more cycles of propagation removed transients. In resonant situations this revealed a charge density that, on further propagation, behaves like a quasistationary (i.e., Floquet) state: it repeats itself (with about 15% loss of norm) after each optical cycle, roughly preserving its shape (duly translated by the quiver motion) during most of the time. A large variety of shapes occur (Fig. 3), and in a nonresonant situation hardly any charge remains. These resonant states turn out to have reasonably well defined parity, and the presense or absence of a node in the symmetry plane perpendicular to the polarization axis in all observed cases was consistent with their excitation by the largest number of photons that did not exceed the shifted threshold.

In some cases (e.g., Fig. 3c) the state looks like a Kramers-Henneberger (KH) state [27] from high-frequency theory [28], with many lobes on the polarization axis [29]. The effects of finite frequency (only about twice the binding energy) are still large, though: while a lobe is far away from the nucleus, its spreads out, to re-contract each time it passes the nucleus [30]. In the high-frequency limit the shape would be completely invariant.

The plateau electrons are produced when on-axis lobes of the resonantly populated states backscatter from the nucleus. Classically, the maximum energy an electron could derive from backscattering out of a bound state (which has zero average velocity) is $8U_p$. In principle the plateau stretches down to zero energy. Below $2U_p$ it is completely masked by direct tunneling, which can happen at any intensity, so that enhancement is not noticeable there.

Some resonant states have a lot of charge density off the polarization axis (e.g., Fig. 3a). They presumably correspond to hitherto unreported highly excited KH states. No resonances due to the lowest KH states were observed, perhaps because the laser frequency is too low compared to their binding energy to make such states stable.

The pure quasistationary states decay faster than expected from the width of the resonance peaks. The system thus cannot be modeled by an excited state coupled to a continuum and a ground state but requires some line narrowing due to destructive interference of common decay modes (light-induced continuum structure [31]). A more detailed discussion of the resonance wave functions and their decay will be presented elsewhere [32].

In conclusion, numerical integration of the Schrödinger equation shows that even in the tunneling regime backscattering is almost exclusively due to resonance enhancement: the charge that tunnels out of the atom near field maxima is trapped by the long-range tail of the Coulomb potential, in an extended but well defined bound state. Thus not only ionization but also excitation can occur through tunneling. The resulting enhancement of ionization should in principle lead to a good peak-valley contrast in this region of the ATI spectrum even in the presence of focal averaging, by the well known mechanism of resonant intensity selection, provided sufficient care is taken to eliminate ponderomotive acceleration of electrons leaving the focus.

This work is part of the research program of FOM (Fundamental Research on Matter), which is subsidized by NWO (Netherlands Organization for the advancement of Research).

[1] P. Agostini, F. Fabre, G. Mainfray, G. Petite and N. K. Rahman, Phys. Rev. Lett. **42**, 1127 (1979).

[2] Ignoring level shifts this happens at $I = U_0^4/16Z^2$, where Z is the final ion charge; S. Augst, D. Strickland, D. Meyerhofer, S. L. Chin, and J. Eberly, Phys. Rev. Lett. **63**, 2212 (1989).

[3] L. V. Keldysh, Sov. Phys. JETP **20**, 1307 (1965).

[4] We use atomic units $m_e = \hbar = e = 1$ unless stated differently.

[5] This is the cycle-averaged kinetic energy a free electron would acquire in the electromagnetic field because of its oscillatory quiver motion.

[6] N. B. Delone and V. P. Krainov, Phys. Usp. **41**, 469 (1998).

[7] B. Walker, B. Sheehy, L. F. DiMauro, P. Agostini, K. J. Schafer, and K. C. Kulander, Phys. Rev. Lett. **73**, 1227 (1994); B. Walker, B. Sheehy, K. C. Kulander, and L. F. DiMauro, Phys. Rev. Lett. **77**, 5031 (1996); B. Sheehy, R. Lafon, M. Widmer, B. Walker, L. F. DiMauro, P. Agostini, and K. C. Kulander, Phys. Rev. A **58**, 3942 (1998).

[8] Creation of higher ionization stages occurs in the tunneling regime, but their ATI spectra are usually masked by those of the neutral.

[9] M. C. Downer, W. M. Wood, and J. I. Trisnadi, Phys. Rev. Lett. **65**, 2832 (1990).

[10] D. G. Lappas and P. L. Knight, Comments At. Mol. Phys. **33**, 237 (1997).

[11] H. G. Muller, A. Tip, and M. J. van der Wiel, J. Phys. B **16**, L679 (1983).

[12] P. H. Bucksbaum, M. Bashkansky, and T. J. McIlrath, Phys. Rev. Lett. **58**, 349 (1987).

[13] J. L. Krause, K. J. Schafer, and K. C. Kulander, Phys. Rev. A **45**, 4998 (1992).

[14] Even half an optical cycle is slow for the atomic ground state, so that it adapts adiabatically if the switching is smooth; the switching was further designed not to alter the drift momentum of free electrons.

[15] K. C. Kulander, K. J. Schafer, and J. L. Krause, in *Atoms in Intense Laser Fields*, edited by M. Gavrila (Academic Press, New York, 1992), p. 247.

[16] H. G. Muller, Laser Phys. **9**, 138 (1999).

[17] H. B. van Linden van den Heuvell and H. G. Muller, *Multiphoton Processes*, Studies in Modern Optics No. 8, edited by S. J. Smith and P. L. Knight (Cambridge University Press, Cambridge, England, 1988).

[18] P. Corkum, Phys. Rev. Lett. **71**, 1994 (1993).

[19] H. R. Reiss, Phys. Rev. A **22**, 1786 (1980).

[20] J. L. Krause, K. J. Schafer, and K. C. Kulander, Phys. Rev. Lett. **68**, 3535 (1992); Phys. Rev. A **45**, 4998 (1992).

[21] G. G. Paulus, W. Nicklich, Huale Xu, P. Lambropoulos, and H. Walther, Phys. Rev. Lett. **72**, 2851 (1994).

[22] M. P. Hertlein, P. H. Bucksbaum, and H. G. Muller, J. Phys. B **30**, L197 (1997).

[23] H. G. Muller and F. C. Kooiman, Phys. Rev. Lett. **81**, 1207 (1998).

[24] R. R. Freeman, P. H. Bucksbaum, H. Milchberg, S. Darack, D. Schumacher, and M. E. Geusic, Phys. Rev. Lett. **59**, 1092 (1987).

[25] According to some definitions of ionization, this is at no time a bound state, just coherently trapped population in the continuum [S. Geltman, J. Phys. B **27**, 257 (1994)].

[26] H. G. Muller, Phys. Rev. A **60**, 1341 (1999).

[27] These are the stationary states bound by the time-averaged potential in the free-electron rest frame [W. C. Henneberger, Phys. Rev. Lett. **21**, 838 (1968)].

[28] M. Gavrila and J. Kaminski, Phys. Rev. Lett. **52**, 613 (1984); M. Pont, N. R. Walet, M. Gavrila, and C. W. McCurdy, Phys. Rev. Lett. **61**, 939 (1988).

[29] M. Gavrila and J. Shertzer, Phys. Rev. A **53**, 3431 (1996).

[30] This contraction is apparent in Fig. 3c, where the rightmost lobe, which passed the nucleus about $1/4$ cycle ago, is much smaller than the (symmetry related) leftmost lobe.

[31] Bonian Dai and P. Lambropulos, Phys. Rev. A **36**, 5205 (1987); P. L. Knight, M. A. Lauder, and B. J. Dalton, Phys. Rep. **190**, 1 (1990).

[32] H. G. Muller, Opt. Express (to be published).